JOURNAL OF GUIDANCE, CONTROL, AND DYNAMICS
Vol. 27, No. 4, July–August 2004

Enhanced Air-to-Air Missile Tracking Using Target Orientation Observations

Yaakov Oshman* and David Arad†
Technion—Israel Institute of Technology, Haifa 32000, Israel

State-of-the-art short-range air-to-air missiles derive their superior interception performance mainly from highly advanced aerodynamic configuration design, agile seekers, and highly efficient fragmentation warheads, but use only relatively basic information on the state of the target. Recent advances in onboard computing and imaging technologies render the expansion of this information base feasible, thus enabling the use of advanced guidance laws. Employing both analysis and computer simulations, this work investigates the idea of enhancing the missile's interception performance by utilizing information on target orientation, acquired in real time by an imaging sensor. Three trackers, including two extended Kalman filters and an interacting multiple model filter, are designed and run in open-loop and closed-loop scenarios to assess and demonstrate the performance enhancement achievable by using the new information. Both proportional navigation and differential-game-based guidance laws are used and compared. The study shows that a great improvement in interception performance can be expected when implementing the proposed concept. Whereas in the case of a missile not exploiting the information on the target's orientation, the required warhead should possess an effective operational radius exceeding 5 m (for the given scenario parameters) even with the advanced, differential-game-based guidance law (and significantly larger with the proportional navigation law); when the new information is used an almost hit-to-kill performance is achieved.

I. Introduction

HIGHLY effective and requiring easily available information, the classical proportional-navigation (PN) guidance law and its variants are extensively used in tactical missiles, including short-range air-to-air missiles (SRAAM).[1] PN renders the missile normal acceleration proportional to the line-of-sight (LOS) rate, commonly measured by an infrared (IR) seeker. Shinar et al.[2] showed that a target can increase the miss distance against a PN-equipped SRAAM by performing hard evasive maneuvers. More advanced guidance laws, such as the augmented-proportional-navigation (APN) law, optimal control guidance law (OGL),[3] or differential game-based laws[4,5] might very well achieve a much smaller miss distance even against a maneuvering target. However, in addition to information provided by traditional LOS rate measurements, advanced guidance laws typically require additional information, comprising the time-to-go, defined as the instantaneous duration remaining until the end of the interception, and the target acceleration.

Target acceleration can be estimated using LOS rate measurements, if a suitable model is assumed for the target dynamics.[6] The common estimation method is based on the well-known Kalman filter (KF) or its extension to nonlinear systems—the extended Kalman filter (EKF). Although KF is the optimal estimator under certain structural and statistical assumptions on the underlying system model, it is nevertheless quite sensitive to uncertainty in its internal model parameters. Target acceleration modeling has been investigated by many researchers. One of the most popular target acceleration models is from Singer.[7] Adapted specifically to manned aircraft, this model assumes that the target acceleration can be described as an exponentially autocorrelated stochastic process. Another approach uses the multiple model adaptive estimator (MMAE) or its variants,[8,9] where the target acceleration is described by a number of models, each based on a different hypothesis. The tasks of the estimator are, in this case, to identify the correct model (i.e., the model that best fits the true target acceleration) online and to provide the guidance system with an accurate estimate of the target state. Thus, Oshman et al.[9] employed an MMAE to deal with a complex scenario involving electronic countermeasures, used by the target to confuse the missile's RADAR seeker.

In practical implementations, the estimation of target acceleration might become prohibitively slow in the presence of noise, rendering the filter's performance characterized by a considerable time lag. In the critical endgame phase of the interception, a time lag too large might result in an unacceptable miss distance, even if the estimator provides an otherwise excellent (but untimely) estimate of the target state. In particular, a maneuvering target is most difficult to track because of the inherent time delay between the time of change of its acceleration and the time when the trajectory of the target reflects this change unambiguously. Thus, when measurements are restricted to the point-mass properties of the target (e.g., LOS measurements) the filter's convergence must be significantly delayed.

The idea underlying the research reported herein is based on the correlation existing between the target's orientation and its evasion maneuvers. In most aerial targets, the target orientation contributes information related to its maneuvers, which might significantly reduce the estimation time delay. This is certainly true for most manned aircraft that use conventional, coordinated bank-to-turn control (but not for vehicles using advanced flight control modes, e.g., direct side-force control). Measurements of target orientation can be obtained from an imaging sensor. Recent developments in imaging sensor technology enable the incorporation of computer vision techniques into seeker heads employing IR or electro-optical sensors, and, thus, facilitate the fusion of target orientation information into the target state estimator. Thus, this work investigates the idea of enhancing the interception performance of an IR seeker-equipped SRAAM by utilizing information on the target orientation (namely, its attitude relative to a missile-fixed coordinate system), acquired in real time by an image processor installed onboard the missile's seeker. The availability and proper processing of target orientation information make it quite conceivable that the estimation of target acceleration and, in particular, the detection of onset of target maneuver will cease to be an issue in the foreseeable future. As previous studies have shown,[9] this might significantly improve the performance of the total guidance system.

Presented as Paper 2001-4110 at the AIAA Guidance, Navigation, and Control Conference, Montreal, Canada, 6–9 August 2001; received 6 December 2001; revision received 3 October 2003; accepted for publication 8 October 2003.

*Associate Professor, Department of Aerospace Engineering; Yaakov.Oshman@technion.ac.il. Associate Fellow AIAA.

†Graduate Student, Department of Aerospace Engineering.

The concept of using imagery data to enhance target tracking performance has been investigated in the past decade in various contexts. Sworder and Hutchins[10] treated the sensor-processor link in a general setting, where an imaging sensor is used to generate a sequence of target images, and an image processor is used to assess the content of each frame and generate a statement about the target and its orientation. In particular, in this work the imaging information about the target's angular orientation was characterized as a marked point process (e.g., a discrete-time Markov process), and the problem was investigated within a probabilistic framework. This probabilistic approach was later used by the same authors in Ref. 11 to investigate the effects of image sensor errors (described by way of a discernibility matrix of probabilities) on the associated target acceleration estimation problem. A two-dimensional simulation study examined the use of this imaging model in the specific context of estimating the acceleration of a land vehicle (tank) engaged in evasive maneuvers. Hutchins and Sworder[12] examined the sensor fusion issues involved in the land-vehicle-tracking scenario, where an imaging sensor was used in combination with a traditional (point mass) sensor to enhance overall tracking performance. A recent important contribution to this field is Ref. 13, in which a unified filtering approach is presented, whereby the optimal minimum mean-square-error filter is derived based on fusing both image-based and conventional (point-mass) measurements. The resulting optimal filter is computationally prohibitive, and the paper proposes a suboptimal alternative in the form of an image-enhanced interacting multiple-model (IMM) filter.

Tracking of a friendly aerial target was investigated in Ref. 14 in the context of air-traffic-control problem. To improve the estimation accuracy of aircraft trajectory while performing a turn, it was suggested to transmit to the ground the aircraft roll angle (as computed by the aircraft's inertial navigation system) via a special transponder device. In Ref. 15 the problem of tracking a friendly aerial target by a chase plane was investigated. The information base consisted of aircraft radar (center of reflection) measurements and a two-dimensional imagery data. A significant improvement in estimation performance was demonstrated up to a very high noise level in the orientation measurement. Andrisani et al.[16] demonstrated how tracking of a maneuvering aircraft (T-38 trainer) from a fixed base can be improved by the processing of its orientation (the three Euler angles). Laneuville and Mariton[17] demonstrated by way of simulation the use of forward-looking-infrared image attributes, such as the number of pixels in the target's image, to detect target maneuver initiation. Shetty and Alouani[18] use imagery data in two ways: detection of a target maneuver using minimal computation and fusing the image centroidal position with a radar measurement. The multisensor system is demonstrated via a simulation assuming image frame size of 512×512. The problem of glint corruption in radar LOS measurement was addressed in Ref. 19, where imaging sensor data were added to the noisy LOS angle radar measurements. The missile's performance was also improved in this work by extracting the target's angle of attack from the target's image and later using it to estimate the target's maneuver. Lawrence[20] also addressed the air-to-air interception problem and stated the idea of using the target orientation as a lead indicator to target maneuver; however, he focused on the image processing aspects of the problem and did not prove the concept.

The common idea investigated in the works just cited is that of using information about the target orientation (generated either by the tracker via imaging, or by the target via its own measurements) to enhance the performance of a target motion estimator. However, a complete investigation of the air-to-air scenario, comprising both the estimation and guidance aspects of the interception of a highly maneuverable evading aircraft by a SRAAM, has not been presented in the context of the works just cited nor has it been investigated, to the best of the authors' knowledge, elsewhere in the open literature. Based on previous related research, however, it is anticipated that, upon becoming mature, the proposed novel technology can lead to significant performance improvements in future SRAAMs.

The remainder of this paper is organized as follows: In the next section, the mathematical model used to analyze the interception problem is stated. An approximate assessment of the measurement noise characterizing the target orientation observation is also presented. A nonlinear observability analysis is presented in Sec. III, which shows the contribution of the orientation observation to the system's observability, relative to the baseline observability rendered by the conventional LOS measurement. Three estimators, designed in this study, are briefly described in Sec. IV. Their open-loop performance is then investigated, in Sec. V, via a Monte Carlo simulation study. The missile's total guidance performance is presented in Sec. VI, using PN and differential game-based guidance laws. Finally, although this work is mainly concerned with the common case of targets performing horizontal evasion maneuvers, the case of a three-dimensional maneuver is also considered, in Sec. VII. Concluding remarks are offered in the final section.

II. Mathematical Model

From the target's point of view, a planar, horizontal maneuver has two clear advantages: 1) the target does not lose kinetic energy while climbing, and 2) a negative-g dive is uncomfortable to the pilot (in the case of a manned target) and limited in intensity. Thus, it is assumed herein that planar, horizontal maneuvers can be used in many cases to model the target's evasive strategy with reasonable accuracy. This assumption is later relaxed in Sec. VII. The kinematical model of the interception problem is formulated in an inertial coordinate system. The coordinate system's origin is in the initial missile's center of gravity, its X_I axis is aligned with the initial LOS, and its Y_I axis is perpendicular to it. The geometry of the endgame scenario is shown in Fig. 1.

Assuming first-order dynamics for both the target and the missile, the nonlinear kinematics and dynamics equations are written in the LOS coordinate system as

$$\dot{R} = V_T \cos(\gamma_T - \lambda) - V_M \cos(\gamma_M - \lambda) \tag{1a}$$

$$R\dot{\lambda} = V_T \sin(\gamma_T - \lambda) - V_M \sin(\gamma_M - \lambda) \tag{1b}$$

$$\dot{\gamma}_M = a_M / V_M \tag{1c}$$

$$\dot{\gamma}_T = a_T / V_T \tag{1d}$$

$$\dot{a}_M = \left(a_M^c - a_M\right) \Big/ \tau_M \tag{1e}$$

$$\dot{a}_T = \left(a_T^c - a_T\right) \Big/ \tau_T \tag{1f}$$

$$\dot{V}_M = 0 \tag{1g}$$

$$\dot{V}_T = 0 \tag{1h}$$

where R is the slant range between the target and the missile; λ is the LOS angle; and $\gamma_M, a_M, V_M, \tau_M$ and $\gamma_T, a_T, V_T, \tau_T$ are the missile and target path angles, accelerations (perpendicular to the respective velocities), speeds, and time constants, respectively. a_M^c and a_T^c are the missile and target acceleration commands, respectively.

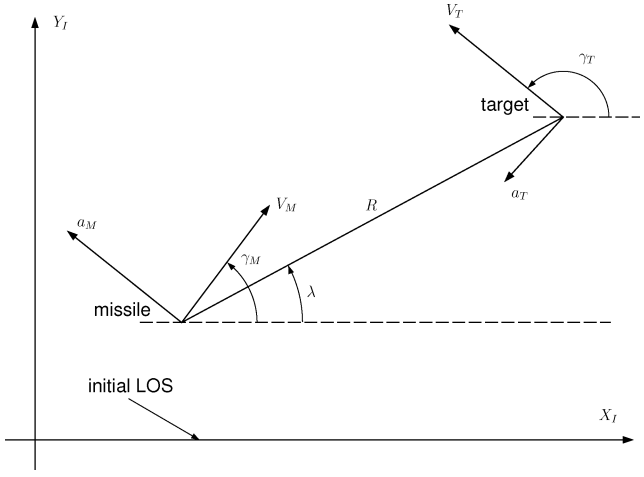

Fig. 1 Endgame scenario geometry.

The missile measurements (normally measured by any IR SRAAM) consist of their own acceleration and velocity and of the LOS angle. These measurements are contaminated by zero-mean white Gaussian noises.

As stated earlier, it is assumed that the target's bank angle ϕ can be measured by the missile IR seeker (via computer vision techniques). Assuming a horizontal coordinated turn, this angle is related to the target acceleration via the equation

$$\phi = \arctan(a_T/g) \tag{2}$$

which is used by the target acceleration estimator (implemented within the missile's autopilot).

To gain an insight on the performance improvement that can be expected by using this measurement, notice that an EKF exploiting this information will be based on the sensitivity derivative

$$\frac{\mathrm{d}\phi}{\mathrm{d}a'_T} = \frac{1}{(a'_T)^2 + 1} \tag{3}$$

where the nondimensional acceleration a'_T is defined as $a'_T \triangleq a_T/g$. Equation (3) shows that the benefit of using the bank-angle measurement decreases as the target evasion acceleration increases. However, it is noted that a constant acceleration maneuver does not, usually, pose a real challenge to the missile guidance system; rather, the more difficult problem (handled by the target acceleration estimator) is to detect timely a maneuver direction switch, and this switch is characterized by a low target acceleration.

A. Imager Measurement Noise

Because target orientation, measured via computer vision techniques, is used by the target acceleration estimator, the inaccuracy of this observation, considered as measurement noise by the estimator, has to be evaluated.

The orientation measurement noise depends on several factors, the most important of which is the type of optics used in the seeker head. In the context of this work, the following two cases are considered.

B. Fixed Field of View

In this case, it is assumed that the imager sees the target with a field of view (FOV), which is fixed for the entire duration of the endgame. This means that the size of the target image (measured in number of pixels) varies throughout the endgame, as the missile approaches the target. This case corresponds to most current seeker heads, which use fixed focal length optics.

The equivalent target orientation measurement noise depends on the size of the imager matrix $m \times m$, the wing span of the target b, the range R, and the FOV angle η. An approximate analysis of an error model for a seeker with a fixed FOV is performed in Ref. 21. For an endgame range of a few kilometers, it is shown there that the relation between the bank-angle error and the range is roughly linear. Assuming a zero orientation error at zero range, the target bank-angle measurement noise is thus assumed in this work to satisfy

$$v_\phi \sim \mathcal{N}\left(0, \sigma_\phi^2\right) \tag{4}$$

with $\sigma_\phi^2 = \kappa^2 R^2$. Taking into account measurement degradation caused by nonperfect head-on or tail-chase intercept and the interference of the tail section, a conservative value for κ is chosen in this work to be 0.25×10^{-3} rad/m.

Remark 1: The target bank angle is bounded because the target is assumed to perform a horizontal turn. Therefore, the imager's orientation measurement noise is bounded, too. This renders the statistical model used in this work, expressed by Eq. (4), rather conservative.

The LOS angle measurement is contaminated, in this case, with white measurement noise

$$v_\lambda \sim \mathcal{N}\left(0, \sigma_\lambda^2\right) \tag{5}$$

In this work a value of $\sigma_\lambda = 1$ mrad was assumed.

C. Variable Field of View

In this case it is assumed that the FOV angle can be varied, such that the size of the target image remains fixed throughout the duration of the endgame. This arrangement can be accomplished, for example, by using a lens with variable focal length in the seeker.

Assume that the target image constantly fills n_i pixels on the image plane. The target bank angle ϕ is calculated based on the coordinates of the target image. An approximate error analysis of the measurement model in this case shows that the bank-angle measurement error is bounded by[21]

$$1/n_i \le |\varepsilon_\phi| \le \sqrt{2}/n_i \tag{6}$$

In this work, the bank-angle measurement noise is conservatively assumed to satisfy

$$v_\phi \sim \mathcal{N}\left(0, \left(\frac{\sqrt{2}}{n_i}\right)^2\right) \tag{7}$$

where v_ϕ is measured in radians.

To assess the LOS measurement noise, notice that the target angular size is $\tan^{-1}(b/R)$. Because the target image fills n_i pixels on the image plane, the LOS angular measurement noise is assumed to satisfy

$$v_\lambda \sim \mathcal{N}\left(0, \left[\tan^{-1}\left(\frac{b}{2n_i R}\right)\right]^2\right) \tag{8}$$

III. Observability Analysis

As is well known, the incorporation of orientation information into a tracking filter will improve the estimation of the target's acceleration. This section presents a nonlinear observability analysis that was carried out in order to evaluate the contribution of the orientation information to the overall observability of the interceptor-evader system, thus providing insight into how the estimator's improved performance is achieved. Following Ref. 22, the method used in this analysis is briefly described in the following:

Consider the nonlinear system

$$\dot{x} = f(x) \tag{9a}$$

$$z = h(x) \tag{9b}$$

where $f : \mathbb{R}^n \to \mathbb{R}^n$ and $h : \mathbb{R}^n \to \mathbb{R}^p$ are vector fields in C^∞. A sufficient condition for system's observability is summarized in the following theorem.

Theorem 1: The system (9) is observable if there exist nonnegative integers $\{l_i\}_1^p$ with $\sum_1^p l_i = n$ such that near the origin of $\mathbb{R}^n$ the matrix

$$\mathcal{O} = \left[\left[L_f^0(\mathrm{d}h_1)\right]^T \ \left[L_f^1(\mathrm{d}h_1)\right]^T \ \cdots \ \left[L_f^{l_1-1}(\mathrm{d}h_1)\right]^T \ \left[L_f^0(\mathrm{d}h_2)\right]^T \ \left[L_f^1(\mathrm{d}h_2)\right]^T \ \cdots \ \left[L_f^{l_2-1}(\mathrm{d}h_2)\right]^T \ \cdots \ \left[L_f^0(\mathrm{d}h_p)\right]^T \ \cdots \ \left[L_f^{l_p-1}(\mathrm{d}h_p)\right]^T\right]^T \tag{10}$$

is nonsingular.

In Eq. (10), $\mathrm{d}h_i$ denotes the gradient of the ith component of h with respect to x. $L_f^1 \mathrm{d}h_i$ is the Lie derivative of $\mathrm{d}h_i$ with respect to f, defined by

$$L_f^1(\mathrm{d}h_i) = L_f\,\mathrm{d}h_i = \left[\frac{\partial(\mathrm{d}h_i)^T}{\partial x} f\right]^T + (\mathrm{d}h_i)\frac{\partial f}{\partial x} \tag{11}$$

where $\partial f/\partial x$ is the Jacobian matrix of f. Also,

$$L_f^0\,\mathrm{d}h_i = \mathrm{d}h_i \tag{12a}$$

$$L_f^k\,\mathrm{d}h_i = L_f\left(L_f^{k-1}\,\mathrm{d}h_i\right) \tag{12b}$$

A. Scenario Analysis

The application of the observability analysis just described to the interception scenario involves tedious computation of Lie derivatives. To facilitate this computation, some simplifications are used. Thus, the missile's velocity, acceleration, and path angle (all directly measurable variables) are assumed known. Moreover, the target acceleration is assumed constant. These assumptions result in the state vector

$$x = [R \quad \lambda \quad \gamma_T \quad a_T \quad V_T]^T \tag{13}$$

with corresponding state equations derived from Eqs. (1).

Depending on the available measurements, the following two cases are investigated.

1. *No Target Orientation Observations*

In this case the measurement equation is

$$h = \lambda \tag{14}$$

and the resulting observability matrix is

$$\mathcal{O}_\lambda = \begin{bmatrix} \left[L_f^0(\mathrm{d}\lambda)\right]^T & \left[L_f^1(\mathrm{d}\lambda)\right]^T & \left[L_f^2(\mathrm{d}\lambda)\right]^T & \left[L_f^3(\mathrm{d}\lambda)\right]^T & \left[L_f^4(\mathrm{d}\lambda)\right]^T \end{bmatrix}^T \tag{15}$$

Explicit expressions for the entries of $\mathcal{O}_\lambda$ are given in Ref. 21.

2. *With Target Orientation Observations*

In this case the measurement equation is

$$h_\phi = [\lambda \quad \phi]^T \tag{16}$$

The observability indices have to satisfy

$$l_\lambda + l_\phi = 5 \tag{17}$$

and the observability matrix is

$$\mathcal{O}_\phi = \begin{bmatrix} \left[L_f^0(\mathrm{d}\phi)\right]^T & \cdots & \left[L_f^{l_\phi-1}(\mathrm{d}\phi)\right]^T & \left[L_f^0(\mathrm{d}\lambda)\right]^T & \cdots & \left[L_f^{l_\lambda-1}(\mathrm{d}\lambda)\right]^T \end{bmatrix}^T \tag{18}$$

Direct computation[21] shows that all Lie derivatives of ϕ with respect to f depend linearly on $\mathrm{d}\phi$ [or $L_f^0(\mathrm{d}\phi)$]. Hence, l_ϕ can be chosen to be either zero or one, resulting in the respective observability matrices:

$$\mathcal{O}_\phi^0 = \begin{bmatrix} \left[L_f^0(\mathrm{d}\lambda)\right]^T & \left[L_f^1(\mathrm{d}\lambda)\right]^T & \left[L_f^2(\mathrm{d}\lambda)\right]^T & \left[L_f^3(\mathrm{d}\lambda)\right]^T & \left[L_f^4(\mathrm{d}\lambda)\right]^T \end{bmatrix}^T \tag{19a}$$

$$\mathcal{O}_\phi^1 = \begin{bmatrix} \left[L_f^0(\mathrm{d}\phi)\right]^T & \left[L_f^0(\mathrm{d}\lambda)\right]^T & \left[L_f^1(\mathrm{d}\lambda)\right]^T & \left[L_f^2(\mathrm{d}\lambda)\right]^T & \left[L_f^3(\mathrm{d}\lambda)\right]^T \end{bmatrix}^T \tag{19b}$$

whose explicit forms are presented in Ref. 21. Either one of these matrices can be used for observability analysis. However, noting that $\mathcal{O}_\phi^0 \equiv \mathcal{O}_\lambda$ and that the bank angle observation only affects $\mathcal{O}_\phi^1$, it is clear that the latter matrix should be investigated for possible observability enhancement relative to the baseline observability contributed by the conventional LOS measurement.

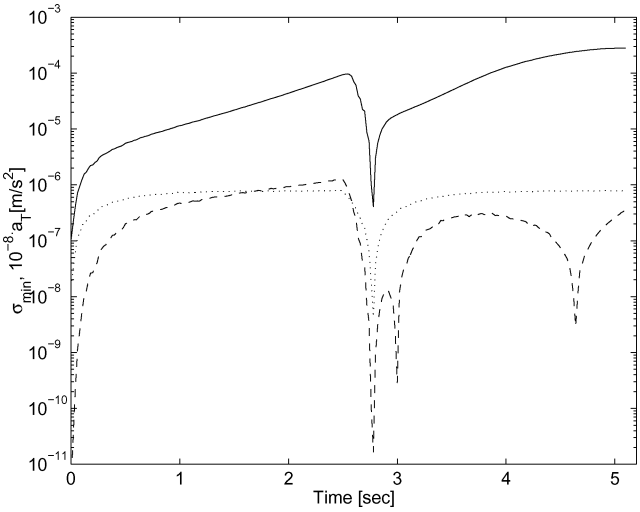

Fig. 2 Smallest singular value of the observability matrix: ——, with orientation measurements; – – –, without orientation measurements; and . . ., target acceleration × 10^{-8}.

B. Numerical Study

A typical head-on interception scenario, detailed in Sec. V, is chosen to investigate the observability of the systems under consideration. The closing velocity is approximately 1000 m/s. Initiated at a range of 5000 m, the intercept lasts approximately 5 s, during which the target performs a bang-bang maneuver.

To quantify the observability enhancement caused by the use of the new orientation measurement, the smallest singular value of the observability matrix, measuring its distance from singularity, is used. Figure 2 shows time histories of the smallest singular values of both observability matrices in a typical scenario. Superimposed on this figure is the magnitude of the target's acceleration, added for reference. Throughout the scenario both observability matrices maintain full rank; however, the effect of the orientation observation on the system's observability is quite substantial, as the smallest singular value is increased by more than two orders of magnitude.

Remark 2: As these results are not related to any particular estimator, they give an excellent indication on the performance enhancement that can be expected from any estimator that judiciously exploits the information contained in the new target maneuver observations.

IV. Target Accleration Estimators

Two EKFs are designed in this study. The first EKF, denoted as EKF-A, assumes that only the regular measurements (i.e., missile's own velocity, acceleration and LOS angle) are available to the missile. The second filter, denoted as EKF-B, is similar to EKF-A, but processes the target orientation measurement as well. An IMM filter, which also processes the target orientation measurement, is designed as well, and its performance is compared with the two EKFs.

A. EKF-A

The filter's state vector is

$$x_f \triangleq [R \quad \lambda \quad \gamma_M \quad \gamma_T \quad a_M \quad a_T \quad V_M \quad V_T]^T \tag{20}$$

The filter dynamics differs from the system dynamics [Eqs. (1)] only by the inclusion of process-noise driving terms in the velocity and acceleration equations

$$\dot{a}_M = \left(a_M^c - a_M\right)\big/\tau_M + \omega_{a_M} \tag{21a}$$

$$\dot{a}_T = -a_T/\tau_T + \omega_{a_T} \tag{21b}$$

$$\dot{V}_M = \omega_{V_M} \tag{21c}$$

$$\dot{V}_T = \omega_{V_T} \tag{21d}$$

Process noise is added to compensate for 1) uncertainty in the velocity and acceleration dynamics and 2) unknown target acceleration command. An estimation performance improvement could be expected if a shaping filter were used to model the target maneuver instead of the white-noise model used herein. Shaping filter requires, however, some characterization of the target maneuver model, which is assumed to be unknown in this work. The process-noise vector thus takes the form

$$\omega = \text{diag}\left\{0, 0, 0, 0, \omega_{a_M}, \omega_{a_T}, \omega_{V_M}, \omega_{V_T}\right\} \tag{22}$$

where ω is a white, zero-mean Gaussian process with power spectral density matrix

$$Q = \text{diag}\left\{0, 0, 0, 0, q_{a_M}, q_{a_T}, q_{V_M}, q_{V_T}\right\} \tag{23}$$

The measurements processed by the filter are the missile's own velocity, acceleration, and LOS angle, which are contaminated by an additive measurement noise according to

$$z = H_x x + v_A \tag{24}$$

with obvious definition of H_x, and where $v_A \sim \mathcal{N}(0, R_A)$ is the white measurement noise sequence with covariance

$$R_A = \text{diag}\left\{r_{a_M}, r_{V_M}, \sigma_\lambda^2\right\} \tag{25}$$

Notice that EKF-A's state equations are nonlinear, calling for a linearization procedure, but its measurement equations are linear. The filter's mechanization is standard and follows Ref. 23.

B. EKF-B

This filter is similar to EKF-A, except that it processes the target orientation measurement in addition to the baseline measurements processed by EKF-A. The measurements processed by the filter are now

$$z = h_B(x) + v_B \tag{26}$$

where

$$h_B(x) = [a_M \quad V_M \quad \lambda \quad \phi]^T \tag{27}$$

and $v_B \sim \mathcal{N}(0, R_B)$ is the white measurement noise sequence with covariance

$$R_B = \text{diag}\left\{r_{a_M}, r_{V_M}, \sigma_\lambda^2, \sigma_\phi^2\right\} \tag{28}$$

Thus, in this case both the state and measurement equations are nonlinear.

C. IMM

The IMM filter[24] assumes that at any point in time the system under consideration obeys one of a finite number of models (modes) and that it can switch between these modes in accordance with a known transition probability matrix. The approach is based on using a filter bank consisting of elemental filters, each tailored to one of the possible modes of the system (i.e., r filters corresponding to r modes or hypotheses on the behavior of the system). At the start of each filtering cycle, the IMM algorithm mixes previous cycle's mode-conditioned estimates and covariances using mixing probabilities computed in the previous cycle. The mixed variables are then used to initialize the elemental filters, which process the measurements to derive the updated estimates, covariances and mode likelihood functions. The likelihood functions then serve to compute the mode probabilities and the mixing probabilities for the next cycle, whereas the updated estimates and covariances serve to compute combined state estimate and covariance. These can be regarded as the outputs of the IMM scheme.

In the case under investigation, each hypothesis (system mode) $M_j(k)$ corresponds at any time instant to a possible target acceleration command. Discretizing uniformly the space of feasible acceleration commands $[-(a_T^c)_{\max}, (a_T^c)_{\max}]$ yields the following set of modes for this problem:

$$M_j = \{[2/(r-1)](j-1) - 1\}\left|\left(a_T^c\right)_{\max}\right| \qquad j = 1, 2, \ldots, N_M \tag{29}$$

where $(a_T^c)_{\max}$ is the assumed maximal target maneuver command and N_M is the number of modes.

The corresponding mode transition probabilities $p_{ij} \triangleq \text{Prob}\{M_j(k)|M_i(k-1)\}$ are conservatively assumed to be equal at each point in time, which means that the filter does not favor any particular maneuver switch over the others. Hence

$$p_{ij} = 1/N_M \qquad \forall i, j \tag{30}$$

The IMM mechanization equations appear in Ref. 24 and are omitted here for brevity.

V. Open-Loop Simulation Study

To assess the estimation performance enhancement achieved by using the new orientation measurement, an open-loop (no guidance) simulation study was carried out. For this purpose, a head-on interception scenario was chosen, where the target performs a single maneuver direction reversal near the middle of the time interval, as shown in Fig. 3. The missile performs no controlled maneuver, flying nearly at its original heading and maintaining seeker lock on target. The endgame starts out at an initial range of 5 km, which is reduced to 518.6 m at the end. The missile and target paths are shown in Fig. 4. The missile and target speeds assume the constant values of $\bar{V}_M$ and $\bar{V}_T$, respectively. The simulation parameters are summarized in Table 1, where γ_{M0} and γ_{T0} are the path angles at the beginning of the endgame.

The three filters use the same initial state estimates and covariance matrix. The true initial state is assumed to satisfy

$$x(t_0) \sim \mathcal{N}(\hat{x}_0, P_0) \tag{31}$$

where the initial estimation error covariance is

$$P_0 = \text{diag}\{50^2, (\pi/180)^2, (3\pi/180)^2, (10\pi/180)^2, 1^2, 10^2, 1^2, 20^2\} \tag{32}$$

with physical units corresponding to the state variables. All filters were driven by measurements acquired at a rate of 50 Hz.

A 100-run Monte Carlo simulation study was performed. Because the missile's guidance system uses the LOS rate and the target acceleration, the estimation performance of these state variables is presented in the sequel for all three filters.

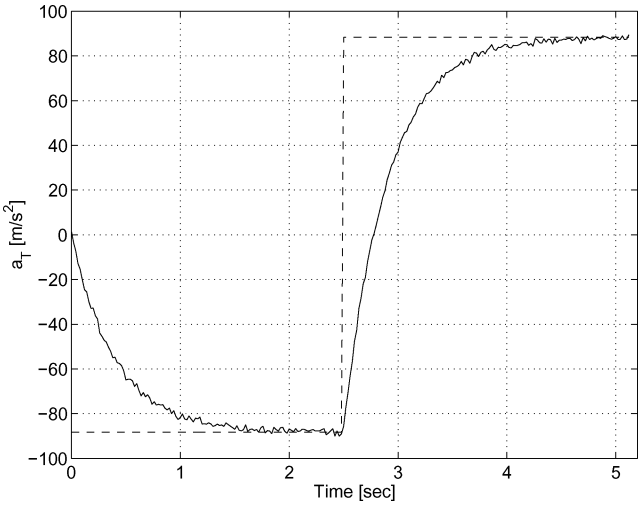

Fig. 3 Target acceleration for open-loop estimation analysis: ——, a_T; and – – –, a_T^c.

Table 1 Simulation parameters

Simulation parameter	Value
R_0, m	5000
λ_0, rad	0
$\bar{V}_M$, m/s	700
$\bar{V}_T$, m/s	300
γ_{M0}, rad	0
γ_{T0}, rad	π
τ_M, s	0.3
τ_T, s	0.4
q_{a_M}, m^2/s^4	1
q_{a_T}, m^2/s^4	1
q_{v_M}, m^2/s^2	1
q_{v_T}, m^2/s^2	1
r_{a_M}, m^2/s^4	1
r_{V_M}, m^2/s^2	1
N_M	11

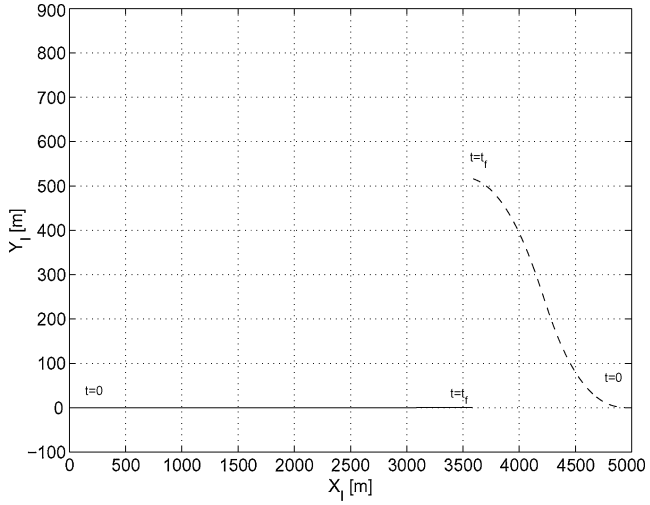

Fig. 4 Trajectories of missile and target in open-loop numerical study: ——, missile and – – –, target.

A. Fixed Field of View

Figures 5–7 present the open-loop estimation performance of the three filters with a conventional seeker having a fixed FOV (FFOV). A 128 × 128-pixel sensor with a 30-deg FOV is assumed. The corresponding bank-angle measurement noise variance varies from 1.56 rad^2 at the beginning of the game, to 0.0168 rad^2 at the end. As can be seen from Figs. 5–7, a major improvement is obtained by using the target orientation measurement (EKF-B) relative to using just the LOS angle (EKF-A), and the IMM filter yields even further improvement.

B. Variable Field of View

Figures 8–10 show the estimation performance obtained with all three filters. An IR imaging seeker with a variable FOV (VFOV) was assumed, such that the target's image size remains about 20 pixels on the imager's 128 × 128 matrix throughout the endgame. This enables a bank-angle measurement with noise variance of about 0.00125 rad^2.

In general, the estimation performance of the VFOV seeker is significantly superior to that of the FFOV seeker. It is clearly seen that, although the EKF-A filter is able to maintain a constant, albeit relatively large, estimation error prior to the target maneuver direction switch (at $t = 2.5$ s), its performance after the switch deteriorates significantly, reaching an acceleration estimation error of about 8 g towards the end of the scenario. This degradation can be attributed to the fact that the LOS angle measurement noise intensity increases as the range to the target decreases [see Eq. (8)]. The LOS angle is estimated better, but its quality gradually decreases as well, as could be expected.

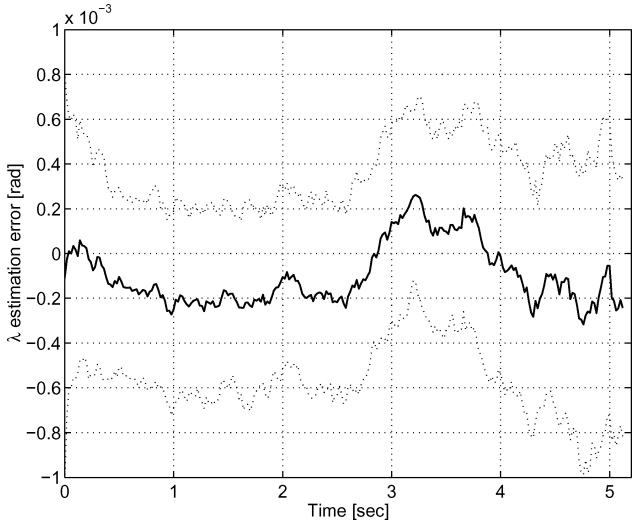

a) LOS angle estimation error

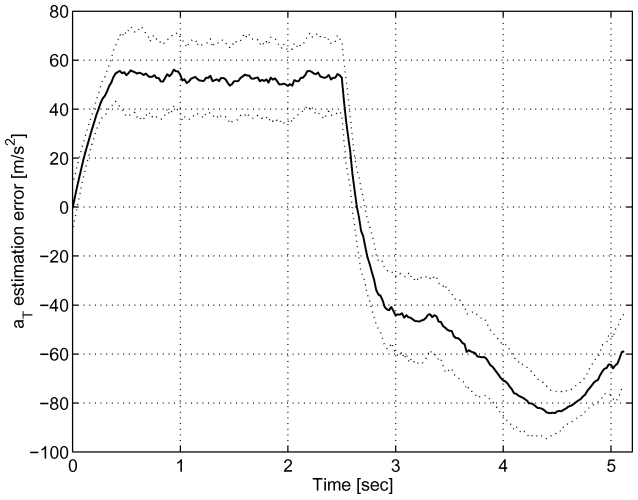

b) Target acceleration estimation error

Fig. 5 EKF-A Monte Carlo FFOV estimation performance: ——, mean error and . . . ., 1-σ envelope.

Upon comparing the performance of the EKF-A and EKF-B filters, it is clear that EKF-B is superior to EKF-A throughout the endgame in estimating both the LOS angle and the target acceleration. Moreover, although EKF-B also exhibits a target maneuver estimation degradation at the maneuver switch time the filter is able to completely recover within only a few tenths of a second.

The more advanced IMM filter generally outperforms the two EKFs. Although it, too, suffers a performance degradation over a short interval starting at the target maneuver switch time, it nevertheless maintains an excellent performance throughout the estimation interval.

Remark 3: For both the EKF-B and IMM filters the acceleration estimation error variance goes to zero soon after the target maneuver direction reversal time (at about 2.8 s, see Figs. 9b and 10b). This can be explained by noting that, from Eq. (3), the largest sensitivity of the target bank angle to the target maneuver occurs when the target maneuver's magnitude is zero. Therefore, the target maneuver estimate benefits the most from the new bank-angle measurement when the target maneuver is zero. Because the maneuver direction switch initiates 2.5 s after the endgame begins, a zero target maneuver occurs at about 2.8 s after the endgame begins. Both EKF-B and IMM filters, which utilize the target's orientation information, derive a highly accurate estimate of the target's maneuver during that time period, as manifested by the low estimation error variance. In contrast, no such phenomenon can be observed in the case of the EKF-A filter, which does not use the target's orientation information (see Fig. 8b).

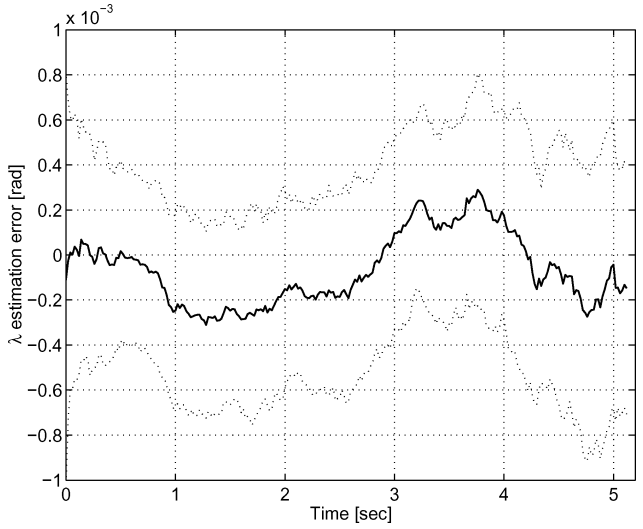

a) LOS angle estimation error

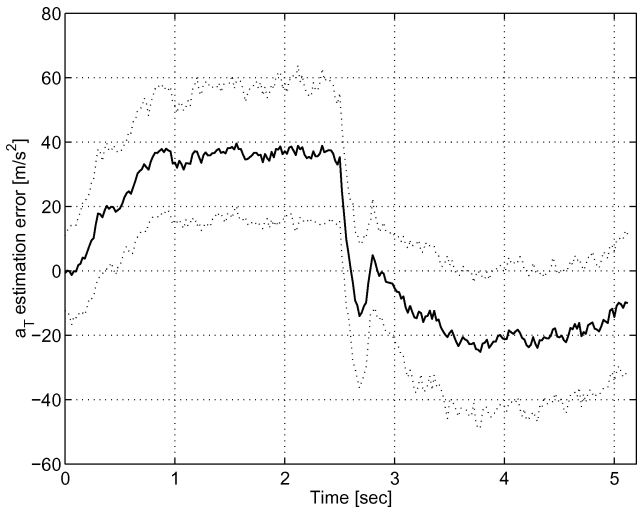

b) Target acceleration estimation error

Fig. 6 EKF-B Monte Carlo FFOV estimation performance: ——, mean error and . . . ., 1-σ envelope.

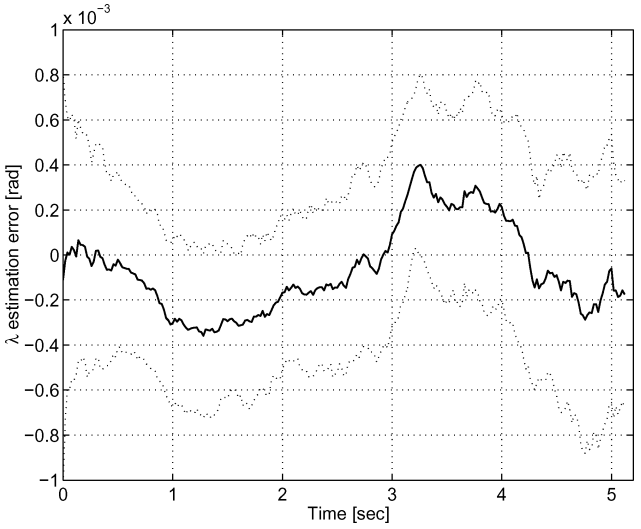

a) LOS angle estimation error

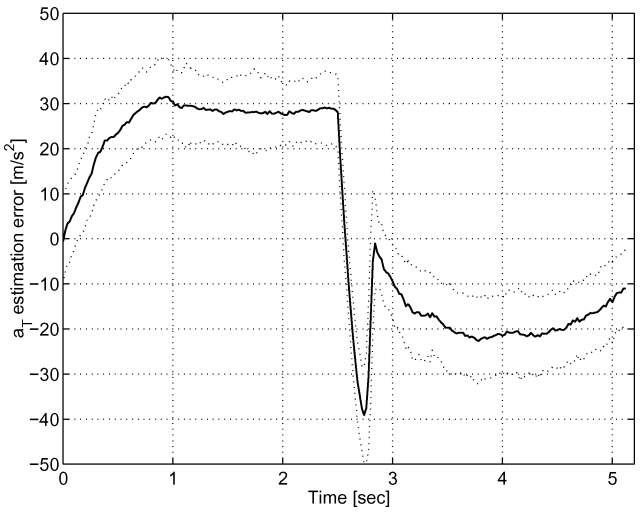

b) Target acceleration estimation error

Fig. 7 IMM Monte Carlo FFOV estimation performance: ——, mean error and . . . ., 1-σ envelope.

VI. Closed-Loop Performance

A Monte Carlo simulation study is carried out to compare the closed-loop estimation performance of the three filters via computing the final miss distance in each case. This comparison is used to investigate the effects of adding the new information to closed-loop systems utilizing various types of guidance laws. In this study, the target performs a hard 9-g bang-bang maneuver, with a maneuver direction reversal time uniformly distributed over the entire endgame interval. The missile's maneuverability is constrained to $a_{M\max} = 20\ g$.

The guidance laws chosen for this study are PN and DGL/1, a differential-game-based law.[5] Both laws assume nothing about future target maneuvers, which makes them better suited to cope with targets performing hard, bang-bang maneuvers than guidance laws such as APN and OGL, which assume a constant target maneuver throughout the endgame. The advanced DGL/1 law represents, in this study, the class of modern guidance laws that require more information (relative to classical laws) on the target's state for their implementation. The performance improvement of the DGL/1 law is compared to that of the PN law, which represents, in this study, the classical class of laws with minimal information requirements. Naturally, because (unlike PN) DGL/1 relies heavily on the target's acceleration estimate it can be expected that its performance improvement when using the enhanced estimators will exceed the corresponding PN performance improvement.

A. PN

The PN guidance law commands the missile to maneuver so as to nullify the LOS rate, placing both the missile and the target on a collision trajectory. The PN law is

$$a_M^c = N' V_c \dot{\lambda} \tag{33}$$

where V_c is the closing velocity and N' is the proportional navigation constant (usually set between three and four). An interesting alternative formulation of the PN law results if it is assumed that the LOS angle is small. In that case, denoting by y the projection along Y_I of the target position relative to the missile, the PN law can be rewritten as

$$a_M^c = \left(1/t_{\rm go}^2\right) N' Z \tag{34}$$

where

$$Z = y + \dot{y} t_{\rm go} \tag{35}$$

is the zero-effort miss (ZEM) distance, which is the miss distance obtained if both the target and the missile do not apply any control until the end of the game, and $t_{\rm go}$ is the time-to-go.

Implementation of PN requires only the LOS angle rate, which is relatively easy to measure, whereas V_c and N' are considered design parameters. In the present study, N' was set to 4, and V_c was set equal to the initial simulation value of 1000 m/s.

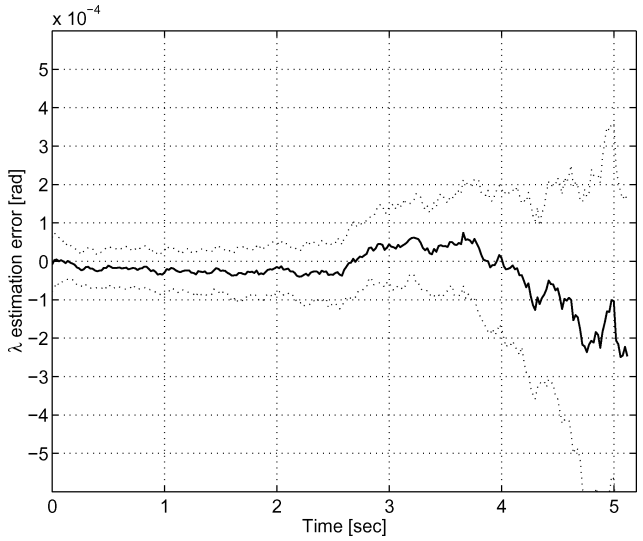

a) LOS angle estimation error

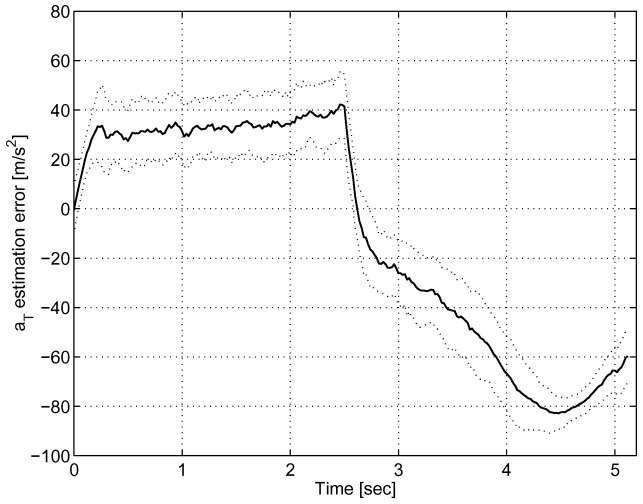

b) Target acceleration estimation error

Fig. 8 EKF-A Monte Carlo VFOV estimation performance: ——, mean error and . . . ., 1-σ envelope.

Figure 11 shows the trajectories of the missile and target in the inertial LOS coordinate frame, in a typical closed-loop endgame scenario. As before, the target maneuver direction reversal time, measured from the beginning of the scenario, is 2.5 s.

An extensive Monte Carlo study was carried out. Most simulation parameters were set identical to those used in the open-loop study. The parameters varying in the closed-loop study were 1) the filters' initial conditions, 2) the process and measurement noise realizations, and 3) the random target maneuver direction reversal time, assumed to be uniformly distributed over the entire endgame duration.

The simulation results are presented in Fig. 12, which shows the cumulative distribution function (CDF) of the miss distance. To assess the closed-loop performance, the warhead is assumed to have an effective operational radius (EOR), defined as the maximal miss distance for which the warhead is effective. Choosing the interception success probability to be 0.95, the required EOR (derived from Fig. 12) is presented in Table 2, which shows that VFOV is clearly superior to FFOV in all filters. Although major reduction of the required EOR is obtained when using the bank-angle information (EKF-B and IMM), it is clear that, in the assumed scenario, an impractical 10-m EOR is required for a 0.95 success probability. To attain this success probability with a warhead of a significantly lower EOR, the missile's maneuverability has to be significantly increased.

Table 2 Required EOR for 0.95 intercept success probability with PN and DGL/1 guidance laws

Seeker/guidance law	EKF-A	EKF-B	IMM
FFOV/PN	19.65	16.10	15.41
VFOV/PN	13.50	10.42	10.13
FFOV/DGL/1	6.19	3.64	2.27
VFOV/DGL/1	5.41	1.03	1.03

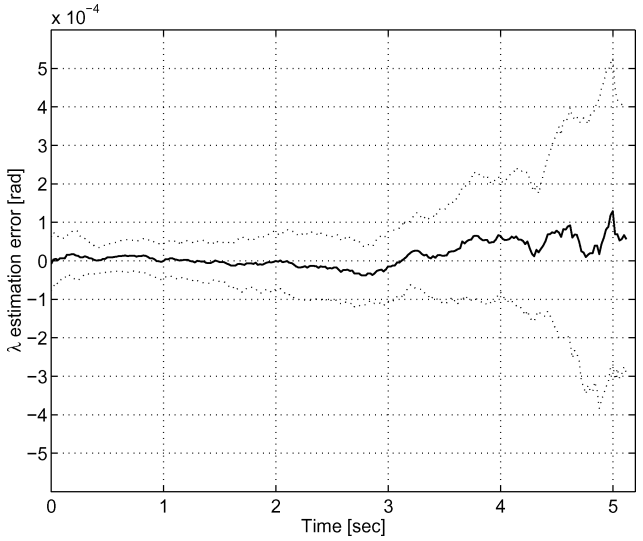

a) LOS angle estimation error

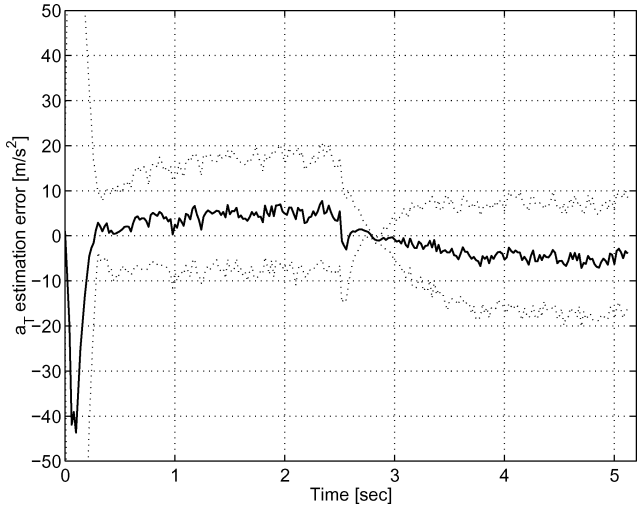

b) Target acceleration estimation error

Fig. 9 EKF-B Monte Carlo VFOV estimation performance: ——, mean error and . . . ., 1-σ envelope.

B. DGL/1

DGL/1 assumes first-order dynamics for both the target maneuver model and the missile. The resulting ZEM is then

$$Z = y + \dot{y}t_{\text{go}} + a_T\tau_T^2\left(e^{-t_{\text{go}}/\tau_T} + t_{\text{go}}/\tau_T - 1\right) - a_M\tau_M^2\left(e^{-t_{\text{go}}/\tau_M} + t_{\text{go}}/\tau_M - 1\right) \tag{36}$$

Based on the solution of a differential game with the miss distance as a performance index, the missile maneuver command is

$$a_M^c = a_{M_{\max}}\text{sign}(Z) \tag{37}$$

The Monte Carlo simulation results for the DGL/1 law are presented in Fig. 13. A comparison of Figs. 12 and 13 shows that, as could be expected, the DGL/1 law makes much better use than the

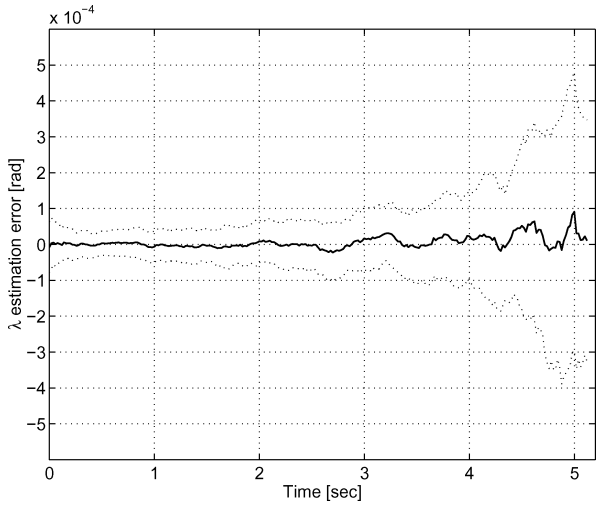

a) LOS angle estimation error

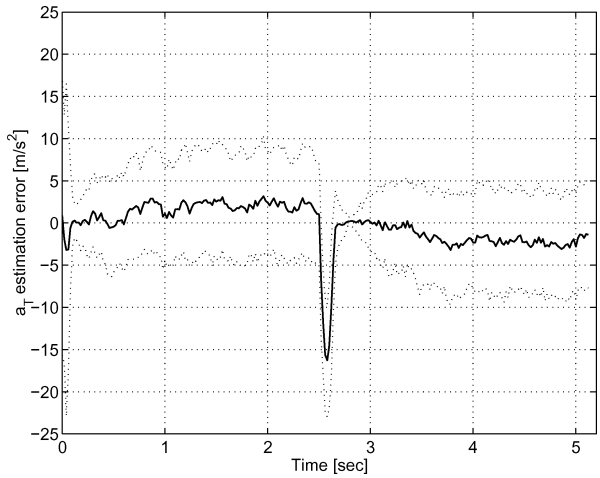

b) Target acceleration estimation error

Fig. 10 IMM Monte Carlo VFOV estimation performance: ——, mean error and . . ., 1-σ envelope.

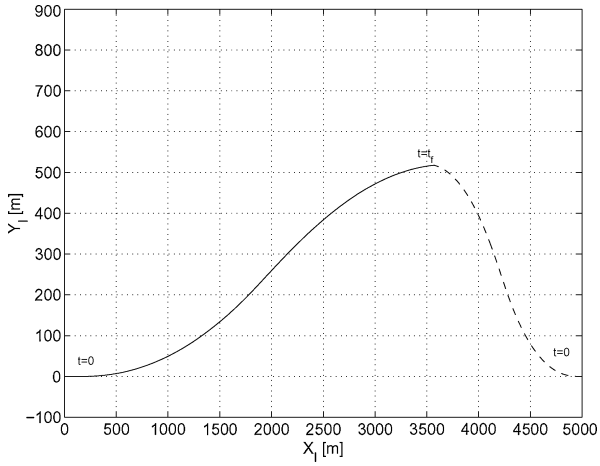

Fig. 11 Typical trajectories of missile and target in close loop numerical study: ——, missile and – – –, target.

PN law of the improved target state estimate, provided to it by the EKF-B and IMM estimators (both utilizing the target's orientation measurements). In fact, PN completely ignores the target acceleration, hence its performance improvement when using the target's orientation information stems only from the enhanced accuracy of the LOS rate's estimate. In contrast, DGL/1 enjoys the improved estimates of both the LOS rate and the target acceleration. Thus, DGL/1 exploits better the new information provided by the imaging seeker.

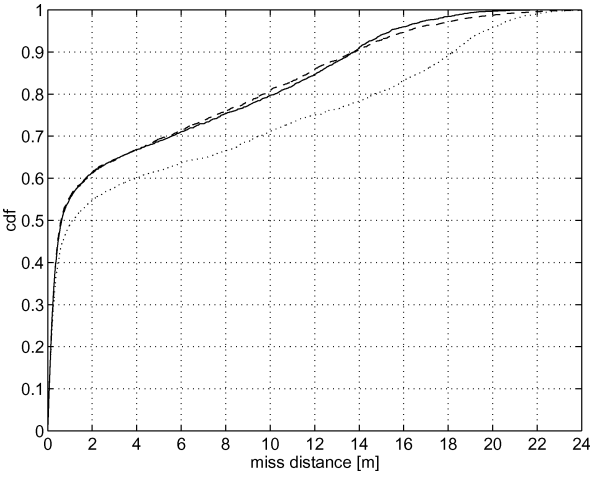

a) FFOV

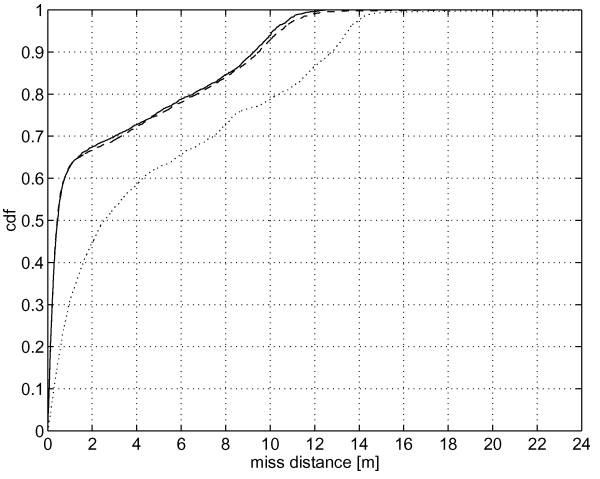

b) VFOV

Fig. 12 PN miss distance CDF: ——, IMM; . . ., EKF-A; and – – –, EKF-B.

Table 2 shows that reasonable EOR values are required for the FFOV seeker, with a minimal value of about 2 m obtained using the IMM filter. The VFOV seeker achieves even better results, practically attaining a hit-to-kill performance with both the EKF-B and the IMM filters. Notice that without using the target orientation measurement, a relatively large EOR is required, even with DGL/1 and a VFOV seeker.

VII. Three-Dimensional Analysis

Although this paper focuses on targets performing planar maneuver, it is nevertheless worthwhile to verify that the missile's performance is not degraded in cases where a three-dimensional maneuver is performed. Thus, this section considers an adaptation of the concept presented earlier to the more general, three-dimensional problem.

A. Mathematical Model

The three-dimensional guidance problem is commonly analyzed by addressing two decoupled planar solutions, namely, a horizontal solution (carried out in a plane perpendicular to Earth's gravity direction) and a vertical solution. The total miss distance is then the root sum square of the horizontal and vertical misses. In the present case, a coupled three-dimensional mathematical model is used, to facilitate the use of the information derived from the imaging sensor.

Modifying the state estimation problem formulation to include the new vertical components results in the following LOS kinematics equations [replacing Eqs. (1a) and (1b)]:

$$\dot{\boldsymbol{R}} = \boldsymbol{V}_T - \boldsymbol{V}_M \tag{38a}$$

$$\boldsymbol{\Omega} = [\boldsymbol{R} \times (\boldsymbol{V}_T - \boldsymbol{V}_M)] \big/ \|\boldsymbol{R}^2\| \tag{38b}$$

where $\boldsymbol{R}$ is the range vector (a vector along the LOS with magnitude equal to the slant range between the missile and the target) and $\boldsymbol{\Omega}$ is the LOS angular velocity vector. The remaining state equations, corresponding to the vertical plane (denoted by subscript v), are

$$\dot{\theta}_M = a_{M_v} \big/ V_M \tag{39a}$$

$$\dot{\theta}_T = a_{T_v} \big/ V_T \tag{39b}$$

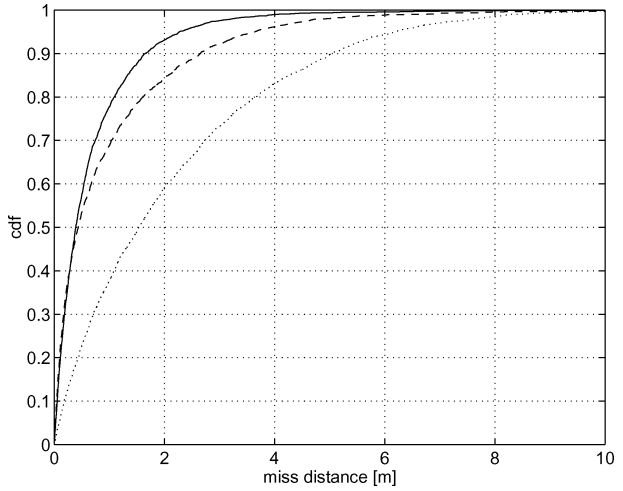

a) FFOV

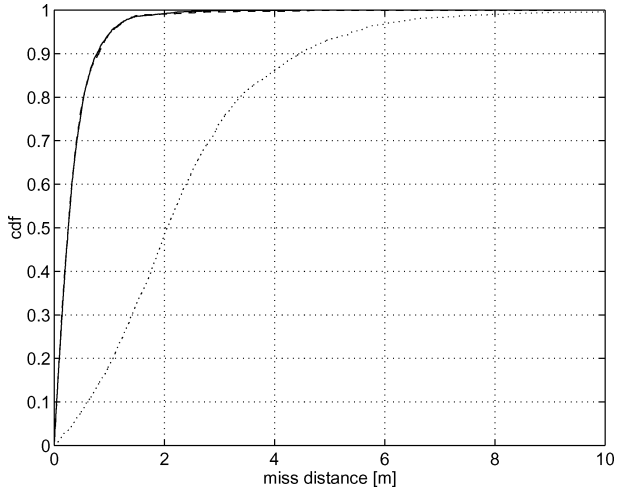

b) VFOV

Fig. 13 DGL/1 miss distance CFD: ——, IMM; . . . ., EKF-A; and – – –, EKF-B.

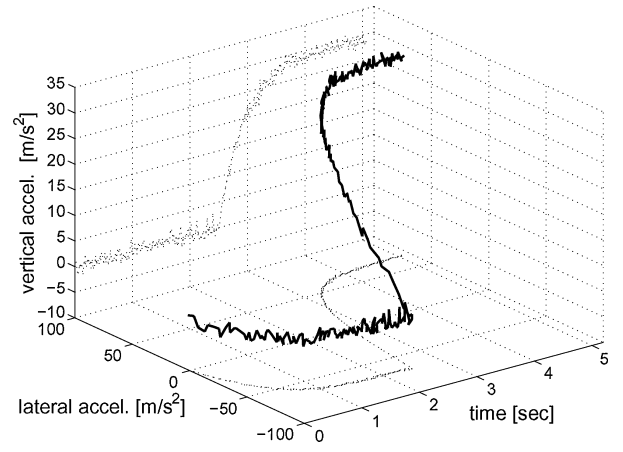

Fig. 14 Target acceleration profile in three-dimensional open-loop simulation.

$$\dot{a}_{M_v} = \left(a^c_{M_v} - a_{M_v}\right) \big/ \tau_M + w_{aM} \tag{39c}$$

$$\dot{a}_{T_v} = \left(a^c_{T_v} - a_{T_v}\right) \big/ \tau_T + w_{aT} \tag{39d}$$

where the definitions of $\theta_M, a_{M_v}, a^c_{M_v}, a_{T_v}$, and $a^c_{T_v}$ follow in an obvious way the definitions of corresponding variables in the horizontal plane. These equations are added to the two-dimensional mathematical model of Eqs. (1) to yield the complete three-dimensional mathematical model.

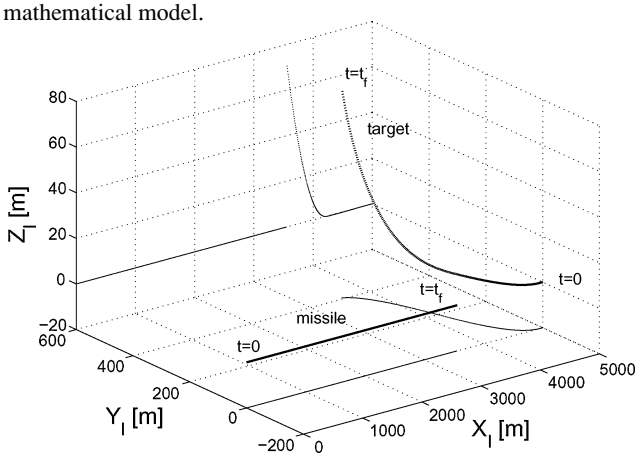

Fig. 15 Trajectories of missile and target in three-dimensional open-loop numerical study: ——, missile and . . . ., target.

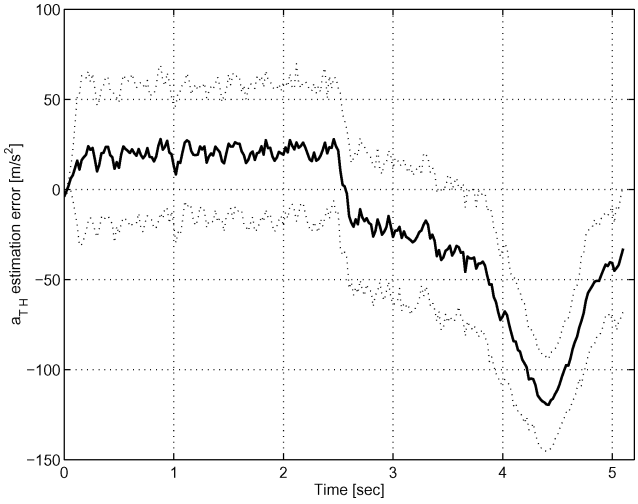

a) Target's horizontal acceleration estimation error

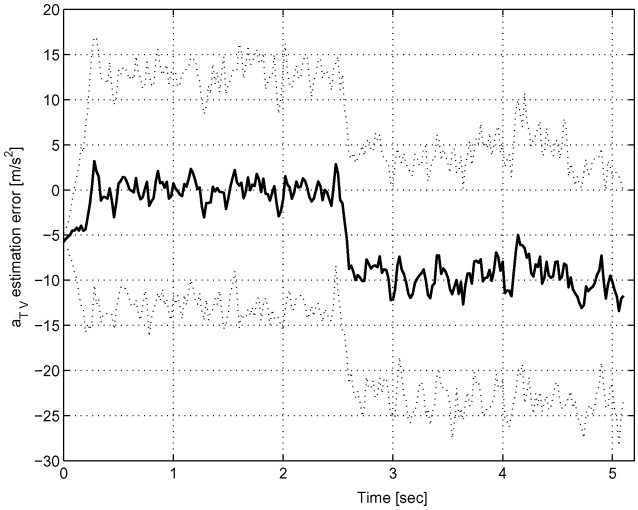

b) Target's vertical acceleration estimation error

Fig. 16 EKF-A Monte Carlo VFOV three-dimensional estimation performance: ——, mean error and . . . ., 1-σ envelope.

In the three-dimensional case the target orientation (bank angle) is related to both the horizontal and vertical components of the target acceleration. In this case Eq. (2) becomes

$$\phi = \arctan\left[a_T \Big/ \left(g + a_{T_v}\right)\right] \tag{40}$$

which expresses the fact that for a pure vertical (pull-up or push-down) maneuver (in which the lateral acceleration a_T is zero) the corresponding bank angle is zero. Likewise, when the maneuver consists of pure lateral acceleration, Eq. (40) reduces to Eq. (2).

B. Simulation Study

To demonstrate the viability of the proposed concept in a typical three-dimensional situation, a head-on interception scenario is chosen. The target performs a single maneuver direction change 2.5 s into the endgame, which lasts about 5 s. The target's maneuver consists of a horizontal maneuver of 7 g (with a direction reversal at the maneuver change time) and a vertical maneuver consisting of a first no-maneuver (0-g) segment lasting up to the direction reversal point and a second steep 3-g pull-up segment throughout the second half of the endgame. As explained earlier, this target maneuver is not advantageous from the target's point of view because of the hard pull-up segment it includes; nevertheless, this maneuver is used here to represent a difficult case from the standpoint of the missile's estimator (which has to estimate the two components of the target acceleration based on the same measurements used in the two-dimensional case). The missile performs no controlled maneuver throughout the scenario (i.e., an open-loop simulation). The endgame starts out at an initial range of 5 km. The target's acceleration profile is shown in Fig. 14. The corresponding target trajectory along with the missile trajectory and their projections on the horizontal and vertical planes are shown in Fig. 15.

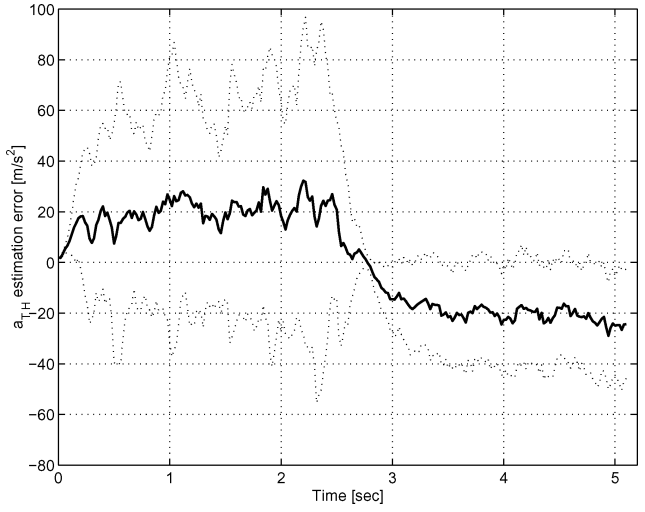

a) Target's horizontal acceleration estimation error

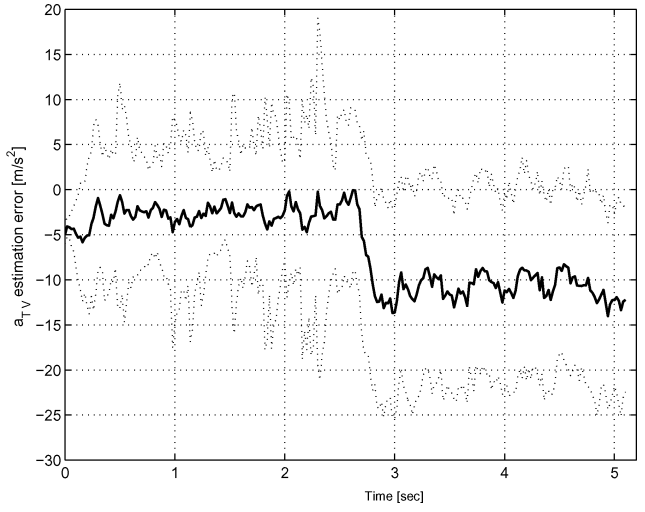

b) Target's vertical acceleration estimation error

Fig. 17 EKF-B Monte Carlo VFOV three-dimensional estimation performance: ——, mean error and . . . ., 1-σ envelope.

The two previously presented EKFs, EKF-A (not using the target orientation measurement) and EKF-B (adapted to process the new target orientation measurement), are used in this study. The mathematical model incorporated in both filters was extended so as to enable the estimation of the two components of the target acceleration in the three-dimensional endgame scenario. The filters' estimation performance is evaluated using the VFOV measurement model. Presenting the estimation performance of both filters in a 100-run Monte Carlo study, Figs. 16 and 17 show that the estimation performance of the filter using the target's bank angle is better than the performance of the filter not using this information. This estimation performance improvement is less dramatic than in the planar case, probably because of the information dilution effect: the same (orientation) measurement is now used to estimate more variables (the two components of the target acceleration). Nevertheless, the performance of the estimator is still satisfactory.

VIII. Conclusions

The concept of using target orientation information to enhance the interception performance of an air-to-air missile is presented, mathematically analyzed, and demonstrated via a Monte Carlo simulation study. Nonlinear analysis is used to evaluate the information contribution of the new measurement to overall system observability. Three estimators, including two extended Kalman filters and an interacting multiple model filter, are designed and used to demonstrate the performance improvement obtained by using the new concept. A Monte Carlo simulation study, including both open-loop scenarios, where no guidance is employed by the missile's autopilot, and closed-loop intercept scenarios, where proportional navigation and differential game-based guidance laws are used, demonstrates that substantial performance improvement can be achieved through better and faster estimation of the target maneuver.

The major conclusion from this study is that using the new concept enables the use of advanced, differential game-based, guidance laws, which normally require an accurate and timely information on the target's acceleration. It is shown that using these guidance laws renders hit-to-kill performance feasible, which can lead to using smaller warheads (or abandoning the use of warheads altogether). The resulting missile can thus be designed smaller, lighter, and with an extended operational range.

It should be emphasized that target orientation information, acquired from an imaging sensor installed onboard the missile's seeker, is not meant to replace conventional line-of-sight measurements. Rather, the new measurement should augment the previously available information. Moreover, it seems feasible that the proposed concept could be implemented in current missiles by adapting present day's technology to the exploitation of additional information from existing sensors.

Acknowledgments

This work was supported by the "Devorah" Fund of the Technion—Israel Institute of Technology. The insightful comments of the anonymous reviewers are gratefully acknowledged.

References

[1]Zarchan, P., *Tactical and Strategic Missile Guidance*, Progress in Astronautics and Aeronautics, Vol. 199, AIAA, Reston, Virginia, 2002, Chap. 8, pp. 143–161.

[2]Shinar, J., Rotsztein, Y., and Bezner, E., "Analysis of Three-Dimensional Optimal Evasion with Linearized Kinematics," *Journal of Guidance, Control, and Dynamics*, Vol. 2, No. 5, 1979, pp. 353–360.

[3]Ben-Asher, J. Z., and Yaesh, I., *Advances in Missile Guidance Theory*, Progress in Astronautics and Aeronautics, Vol. 180, AIAA, Reston, VA, 1998, Chap. 3.

[4]Gutman, S., "On Optimal Guidance for Homing Missiles," *Journal of Guidance and Control*, Vol. 2, No. 4, 1979, pp. 296–300.

[5]Shinar, J., "Solution Techniques for Realistic Pursuit-Evasion Games," *Advances in Control and Dynamic Systems*, edited by C. T. Leondes, Vol. 17, Academic Press, New York, 1981, pp. 63–124.

[6]Chang, C. B., and Tabaczynski, J. A., "Application of State Estimation to Target Tracking," *IEEE Transactions on Automatic Control*, Vol. AC-29, No. 2, 1984, pp. 98–109.

[7]Singer, R. A., "Estimating Optimal Tracking Filter Performance for Manned Maneuvering Targets," *IEEE Transactions on Aerospace and Electronic Systems*, Vol. AES-6, No. 4, 1970, pp. 473–483.

[8]Hexner, G., Weiss, H., and Dror, S., "Temporal Multiple Model Estimator for a Maneuvering Target," Dept. of Aerospace Engineering, TAE Report 859, Technion—Israel Inst. of Technology, Haifa, Israel, Feb. 2001.

[9]Oshman, Y., Shinar, J., and Avrashi-Weizman, S., "Using a Multiple Model Adaptive Estimator in a Random Evasion Missile/Aircraft Encounter," *Journal of Guidance, Control, and Dynamics*, Vol. 24, No. 6, 2001, pp. 1176–1186.

[10]Sworder, D. D., and Hutchins, R. G., "Image-Enhanced Tracking," *IEEE Transactions on Aerospace and Electronic Systems*, Vol. 25, No. 5, 1989, pp. 701–709.

[11]Sworder, D. D., and Hutchins, R. G., "Maneuver Estimation Using Measurements of Orientation," *IEEE Transactions on Aerospace and Electronic Systems*, Vol. 26, No. 4, 1990, pp. 625–638.

[12]Hutchins, R. G., and Sworder, D. D., "Image Fusion Algorithms for Tracking Maneuvering Targets," *Journal of Guidance, Control, and Dynamics*, Vol. 15, No. 1, 1992, pp. 175–184.

[13]Evans, J. S., and Evans, R. J., "Image-Enhanced Multiple Model Tracking," *Automatica*, Vol. 35, No. 11, 1999, pp. 1769–1786.

[14]Lefas, C. C., "Using Roll-Angle Measurements to Track Aircraft Maneuvers," *IEEE Transactions on Aerospace and Electronic Systems*, Vol. AES-20, No. 6, 1984, pp. 672–681.

[15]Kendrick, J. D., Maybeck, P. S., and Reid, J. G., "Estimation of Aircraft Target Motion Using Orientation Measurements," *IEEE Transactions on Aerospace and Electronic Systems*, Vol. AES-17, No. 2, 1981, pp. 254–259.

[16]Andrisani, D., Kuhl, F. P., and Gleason, D., "A Nonlinear Tracker Using Attitude Measurements," *IEEE Transactions on Aerospace and Electronic Systems*, Vol. AES-22, No. 5, 1986, pp. 533–538.

[17]Laneuville, D. and Mariton, M., "Image Based Target Maneuver Detection," *IEEE Proceedings of the 30th Conference on Decision and Control*, Vol. 2, IEEE Press, Piscataway, NJ, 1991, pp. 2066, 2067.

[18]Shetty, S., and Alouani, A. T., "A Multisensor Tracking System with an Image-Based Maneuver Detector," *IEEE Transactions on Aerospace and Electronic Systems*, Vol. 32, No. 1, 1996, pp. 167–181.

[19]Uhrmeister, B., "Kalman Filters for a Missile with Radar and/or Imaging Sensor," *Journal of Guidance, Control, and Dynamics*, Vol. 17, No. 6, 1994, pp. 1339–1344.

[20]Lawrence, R. V., "Precision Guidance Against Manoeuvring Targets," *Proceedings of the American Control Conference*, Vol. 6, IEEE Press, Piscataway, NJ, 1995, pp. 4127–4130.

[21]Arad, D., "Improving the Interception Performance of Air to Air Missiles Using Target Orientation Information," M.S. Thesis, Technion—Israel Inst. of Technology, Dept. of Aerospace Engineering, Haifa, Nov. 2001.

[22]Krener, A. J., and Respondek, W., "Nonlinear Observers with Linearizable Error Dynamics," *SIAM Journal of Control and Optimization*, Vol. 23, No. 2, 1985, pp. 197–215.

[23]Jazwinski, A. H., *Stochastic Processes and Filtering Theory*, Academic Press, New York, 1970, Chap. 8, p. 278.

[24]Blom, H. A. P., and Bar-Shalom, Y., "The Interacting Multiple Model Algorithm for Systems with Markovian Switching Coefficients," *IEEE Transactions on Automatic Control*, Vol. 33, No. 8, 1988, pp. 780–783.